Buoyancy Suppression in Gases at High Temperatures

Maria A. Kuczmarski*, Suleyman A. Gokoglu

NASA Glenn Research Center, 21000 Brookpark Road, Cleveland, OH 44135

Abstract

The computational fluid dynamics code FLUENT was used to study Rayleigh instability at large temperature differences in a sealed gas-filled enclosure with a cold top surface and a heated bottom wall (Bénard problem). Both steady state and transient calculations were performed. The results define the boundaries of instability in a system depending on the geometry, temperature and pressure. It is shown that regardless of how fast the bottom-wall temperature can be ramped up to minimize the time spent in the unstable region of fluid motion, the eventual stability of the system depends on the prevailing final pressure after steady state has been reached. Calculations also show that the final state of the system can be different depending on whether the result is obtained via a steady-state solution or is reached by transient calculations. Changes in the slope of the pressure-versus-time curve are found to be a very good indicator of changes in the flow patterns in the system.

Keywords: buoyancy, natural convection, numerical modeling, Bénard problem

---

* Corresponding author. Tel.: +1 216 433 3651; fax: +1 216 433-3651

E-mail address: Maria.A.Kuczmarski@nasa.gov (M. Kuczmarski)

Nomenclature

C_p	heat capacity at constant pressure (kJ/kg K)
g	gravitational constant (m/s^2)
Gr	Grashof number (dimensionless)
k	thermal conductivity (W/m K)
L	characteristic length (m)
P	pressure (atm)
P_i	initial pressure (atm)
P_f	final pressure (atm)
Pr	Prandtl number (dimensionless)
Q	total heat transfer rate (J/s)
Ra	Rayleigh number (dimensionless)
Ra_c	critical Rayleigh number (dimensionless)
T	temperature (K)
$\overline{T}$	average temperature (K)
T_c	cold-wall temperature (K)
T_h	hot-wall temperature (K)
T_i	initial temperature (K)
V_{max}	maximum velocity (m/s)

Greeks

α	thermal diffusivity (m^2/s)
β_T	coefficient of thermal expansion at constant pressure (K^{-1})
μ	dynamic viscosity (kg/m s)
ν	kinematic viscosity (m^2/s)
ρ	density (kg/m^3)
ρ_i	initial density (kg/m^3)

1. Introduction

When a horizontal enclosed space is heated to a uniform bottom-wall temperature greater than that of the top wall, an upwardly decreasing temperature profile is established. For a sufficiently small temperature difference between the bottom and top walls, viscous forces are greater than buoyancy forces, and the fluid remains quiescent. However, as this temperature difference increases, a point will be reached at which the buoyancy forces will become greater than the viscous forces, and the fluid begins to move. This is known as the classic Bénard problem.

The Rayleigh number is used to define the onset and development of buoyant flow under these conditions. It is defined as:

$$Ra \equiv \frac{(\rho_i - \rho)}{\rho_i} \frac{gL^3}{\alpha \nu} \tag{1}$$

where

$$\nu = \frac{\mu}{\rho} \tag{2}$$

The Rayleigh number can also be expressed as the product of the Grashof number, Gr, and the Prandtl number, Pr:

$$Ra = Gr \times \mathrm{Pr} \tag{3}$$

where

$$Gr \equiv \frac{(\rho_i - \rho)}{\rho_i} \frac{gL^3}{\nu^2} \tag{4}$$

and

$$\mathrm{Pr} \equiv \frac{\nu}{\alpha} = \frac{\mu C_P}{k} \tag{5}$$

The fluid remains stable if the Rayleigh number is less than the critical Rayleigh number, Ra_c. Once the critical Rayleigh number is exceeded, finger-like intrusions of the lighter gas into the heavier gas and the heavier gas into the lighter gas result. Goldstein and Volvino (1995) have presented a summary of various investigations in the literature for the onset of convection and flow development in horizontal layers. Widely ranging values of the critical Rayleigh number were reported, anywhere from 1000 to 3000.

While the above studies used different criteria and different experimental observations as the basis for determining the onset of instability, one possible explanation for this wide range of values is that the Rayleigh and Grashof numbers are derived assuming the Boussinesq approximation. This assumes that all fluid properties are constant, except for density in the buoyancy term of the momentum equation, and that viscous dissipation can be neglected (Kays and Crawford, 1980). Under these conditions, the density difference can be approximated as:

$$\frac{(\rho_i - \rho)}{\rho_i} = \beta_T (T - Ti) \tag{6}$$

where

$$\beta_T = -\left(\frac{1}{\rho}\right) \times \left(\frac{\partial \rho}{\partial T}\right)_P \tag{7}$$

which is the coefficient of thermal expansion at constant pressure.

While the temperature dependence of thermodynamic and transport properties can often be safely neglected at small temperature differences, they become important at large

temperature differences and their effects must be included in order to obtain accurate descriptions of the state of flow inside the enclosure. This is particularly true for gases, which tend to become more stable at higher temperature differences due to the dampening effect of gas viscosity at high temperatures. Under non-Boussinesq conditions, the predictive abilities of dimensionless numbers derived by assuming Boussinesq conditions require more attention. Gray and Giorgini (1976) and Paolucci and Chenoweth (1987) reported on the validity of the Boussinesq approximation and departures from it. These studies led to the specification of conditions under which it is justified to neglect certain terms in the Boussinesq approximation.

In a previous paper, Gokoglu and Kuczmarski (2003) showed via a steady state analysis that for temperature differences larger than justifiable for the Boussinesq approximation, there are situations were a gaseous system will never experience the onset of buoyant convection, no matter how large the temperature difference becomes at a given pressure. This was due to the temperature-dependent gas properties, particularly that of the kinematic viscosity, which tended to counteract the tendency toward instability at higher temperatures. In addition, two critical hot surface temperatures were shown to exist for a given pressure, above and below which the system was stable.

In this paper, transient calculations have been performed to examine the behavior of the system as it pressurizes while the bottom wall is heated at different rates. These transient solutions are carried out over a sufficiently long time period to allow comparison between results obtained from transient solutions and those obtained using steady-state solutions at the final prevailing pressure. The development of the flow field over time for

different heating rates and its effect on the temperature field is demonstrated. In addition, the effect of varying the enclosure height on the predicted range of instability is examined.

2. Numerical Models

This investigation used the computational fluid dynamics code FLUENT, which uses a finite volume method to discretize the continuity, momentum, and energy equations. Two 2-D models of a rectangular geometry were constructed, as shown in Fig. 1. Case 2 has a distance between the hot and cold walls that is twice that of case 1. Adiabatic boundary conditions were set along both side walls, and the top cold-surface temperature was set at 300 K. The bottom hot-surface temperature was set at 2500 K for the steady state cases, or ramped to a final temperature of 2500 K for the transient cases. Neon gas was used in the enclosure. For the steady-state cases, the operating pressure was defined, along with a hot-wall temperature of 2500 K. The standard discretization scheme in FLUENT was used for pressure and the SIMPLE algorithm for the pressure-velocity coupling. A second order upwind scheme was used for the continuity, momentum, and energy equations. For the transient calculations, an initial pressure was specified, but a floating operating pressure was defined in the model to allow the pressure to increase as the gas was heated. A second order upwind scheme was used for the momentum and energy equations, and for the density interpolation scheme. The PRESTO! discretization scheme was used for pressure, and the PISO algorithm was employed for the pressure-velocity coupling. A second order upwind scheme was used for the continuity, momentum, and energy equations. A time step of $1x10^{-4}$ second was used for all transient calculations. Larger time steps led to problems with convergence. The under-relaxation factors were set

to 1 for pressure, density, body forces, momentum, and energy. This helped speed the computations that were slowed by the necessity of choosing a small time step. The solutions were considered converged for steady state solutions when the scaled residuals dropped below $1x10^{-3}$ for the continuity equation, $1x10^{-5}$ for the momentum equations, and $1x10^{-6}$ for the energy equation. Convergence for the transient solutions required these values to be obtained for each time step. All transient cases were run up to ten seconds.

Four different grid densities were examined for case 1 to study the solution grid sensitivity. The total heat transfer rate at the heated bottom wall was compared among the four grids, since this heat transfer into the system was the ultimate source for all changes experienced by the system. Table 1 shows the number of computational cells used for each grid, along with the total heat transfer rate at the bottom wall, Q, and the change in this rate between consecutive grids. The change in the total heat transfer rate is of the same order of magnitude between grids 1 and 2 as it is between grids 2 and 3; both are at very small values. Because the computational time increases with the grid density, grid 2 was chosen to balance higher resolution with reasonable run times. All results in the rest of this paper for case 1 were obtained using grid 2.

For case 2, the grid used was based on grid 2 discussed above. The number of computational cells in the X-direction remained the same at 240 cells, but the number of computational cells in the Y-direction was simply doubled from 40 cells to 80 cells since the height of case 2 is double that of case 1.

3. Results

First, the upper and lower temperature limits on stability were determined for the two cases with different enclosure heights by running steady-state cases at various pressure levels. The results are shown in Fig. 2. It can be seen that regardless of the temperature difference, some systems always remain stable below a certain minimum pressure, depending on the height of the geometry. Neon was stable for all hot-surface temperatures at 1 atm of pressure or less for case 1, but the pressure needed to be decreased to 0.36 atm or less in case 2 before neon was stable at all hot-surface temperatures. In addition, the range of pressures and temperatures for which the system is unstable is expectedly much greater for case 2 than for case 1 since the characteristic length, i.e., the height between the top and bottom walls in this study, is doubled in case 2, resulting in an eight-fold increase in the Rayleigh number. These results also confirm the original findings of Gokoglu and Kuczmarski (2003) that the tendency of a system to become more unstable can actually decrease when hot-surface temperature is increased beyond a certain level where the dampening effect of gas viscosity becomes more prevalent.

Next, transient runs were conducted to examine the behavior of the system as it dynamically develops. The same scales were used for Figs. 8-17, i.e., a range of $2x10^{-8}$ to $5x10^{-1}$ m/s for velocity and a range of 300 to 2500K for temperature. The curves showing the rise in pressure with the bottom-wall temperature are plotted in Figs. 3 and 4 for both cases at initial pressures of 1.0 and 1.5 atm. The bottom-wall temperature was ramped to a final temperature of 2500 K over 0.1, 0.5, 1.0, and 5.0 seconds. The curves are superimposed over the results obtained from steady-state calculations showing the stable and unstable regions. For all ramp times, the system crosses over into the unstable region

at least part of the time. For case 1, at an initial pressure of 1 atm, all cases cross back over to the stable region at the end of the ramp, although they remain very close to the transition line. For case 2, at an initial pressure of 1 atm, the system quickly crosses into the unstable region and remains there for the 0.5, 1.0, and 5.0 second ramp times. For the 0.1 second ramp time, the curve crosses over into the stable region again, but after the final hot-wall temperature is reached, the pressure continues to rise towards its steady state, and the system ends up back in the unstable region. So, even though the bottom-wall temperature can be ramped at a rate that causes the system to undergo a stable-unstable-stable transition, the system will eventually end up in a region defined by the final pressure the system rises to. This pressure can be estimated using the ideal gas law:

$$P_f = \frac{nRT}{\mathrm{V}} \tag{8}$$

The number of moles of gas in the system can be determined from the initial conditions, but the temperature to use in this equation is not as obvious. The arithmetic mean of the hot- and cold-wall temperatures in the system, customarily used to evaluate gas properties, can be used (Kays and Crawford, 1980; Bird, Stewart, and Lightfoot, 1963):

$$\overline{T} = \frac{T_h + T_c}{2} \tag{9}$$

Table 2 shows the final system pressure calculated from equation (8), the pressure predicted by FLUENT at 10 seconds, and the percent differences between the two, determined by the equation:

$$\%difference = \left(\frac{P_{f,FLUENT} - P_{f,ideal\_gas\_law}}{P_{f,ideal\_gas\_law}} \right) \times 100 \tag{10}$$

The largest difference observed is less than 15%, a relatively close agreement.

The pressure rise with time for various bottom-wall temperature ramp rates is shown in Figs. 5 and 6. A change in the slope of the curve is a good indicator of a change in the flow field. This is most clearly illustrated in Fig. 6b for case 2, with an initial pressure of 1.5 atm and a bottom-wall temperature ramp rate of 5.0 sec. At around the five second mark, the pressure curve changes from a steady rise to a brief plateau. Fig. 7a shows this region in more detail with higher resolution. During about a 0.6-second interval where the pressure drops, Fig. 7b – 7e shows the transition in the velocity field from six convective cells down to four. An accompanying change in heat transfer rates and temperature in the enclosure causes the observed change in the pressure curve. This observation can be a convenient experimental tool for diagnosing the expected changes in flow behavior in such systems.

Regarding case 1, it was shown in Fig. 3(a) that the pressure vs. hot-wall temperature curves end up in the stable region near the transition between unstable and stable flow for all hot-wall temperature ramp times investigated. This stability map was obtained using steady-state calculations. Fig. 8 shows that when a transient solution is obtained, convective rolls are predicted to be present in the system for the 0.1 and 0.5 sec. ramp times. However, the velocity is at such low values at selected times during the transient run that the temperature fields are not significantly affected. This is in contrast to the results obtained from a transient solution shown in Fig. 9. Convective rolls are predicted to be present at a sufficient strength to affect the temperature fields. In both figures, the transient solution is seen to no longer be changing at ten seconds, indicating that a steady state has been reached. It can be seen that the transient results at ten seconds

are different than those predicted by the steady state solution, pointing out that a transient solution may be necessary to accurately predict the final state of a system such as this. Figs. 10 and 11 show similar results between the steady-state analysis and the transient calculations carried out to ten seconds. Compared to the cases with an initial pressure of 1 atm, these cases with the initial pressure of 1.5 atm show a much greater effect on the temperature field from the velocity field.

Regarding case 2, Figs. 12, 13, and 14 show that the greater height in case 2 has led to higher velocities compared to case 1, with a corresponding effect in the temperature field. Similar results for an initial pressure of 1.5 atm are shown in Figs. 15, 16, and 17. At an initial pressure of 1 atm, the number and/or size of the predicted convective rolls is different between the steady-state solution and the transient solution taken out to ten seconds. For the cases with an initial pressure of 1.5 atm, on the other hand, steady-state calculations can sometimes predict the final state of the system consistently with the transient calculations. Such discrepancies between steady-state and transient calculations points out again that the history of the development of flow structures and their corresponding temperature fields have a profound effect on the eventual final state which can not be properly captured by only steady-state calculations.

4. Conclusions

This study demonstrated a capability to define the range of instability in a gaseous enclosed system depending on its geometry, temperature, and pressure. It is shown by transient calculations that while the bottom-wall temperature can be ramped fast enough to minimize the time spent in the unstable region of fluid motion, the final state of the system

depends on the final pressure eventually attained after steady state has been reached. The results also show that steady-state and transient solutions can give different results as to the final state of the system indicating that the history of the development of flow instabilities is important and that steady-state calculations can not always be relied upon. It is also demonstrated that changes in the monotonic behavior of the pressure versus time curve in a transient treatment of the problem is a good indicator of changes in flow patterns in the system and can also be used as an experimental diagnostic tool.

Many applications involving heat transfer in gaseous media, such as chemical vapor deposition, combustion, and cryogenics, require knowledge of the onset of convective instability in order to design systems to perform as needed. This work has shown that high temperatures can be effectively used to actually *suppress* buoyant convection in gaseous systems utilizing the enhanced dampening effect of increased gas viscosities. Using existing heat transfer correlations involving the Rayleigh and Grashof numbers under conditions where the Boussinesq approximation is no longer valid, a common practice, could be seriously misleading since the system stability can not correctly be predicted by these dimensionless numbers. In addition, the intensity of the buoyant convection can be misjudged by not considering the history of the system during heating. Depending on the system conditions, the temperature dependent properties of the gas must be included to fully understand the heat transfer occurring in the system.

5. Acknowledgements

This work was supported by the Microgravity Combustion Science Program in the Office of Biological and Physical Research at NASA.

6. References

Bird, R.B., Stewart, W.E., Lightfoot, E.N., 1960, Transport Phenomena, John Wiley & Sons, New York, NY.

Gokoglu, S.A., Kuczmarski, M.A., 2003. Suppression of Buoyancy in Gaseous Media at High Temperatures. In: Proceedings of the Fourth International Symposium on Scale Modeling, Cleveland, Ohio, USA, 2003, pp. 74-84.

Goldstein, R.J., Volino, R.J., 1995. Onset and Development of Natural Convection above a Suddenly Heated Horizontal Surface. Journal of Heat Transfer, 117, pp. 808-821.

Gray, D.D., Giorgini, 1976. The Validity of the Boussinesq Approximation for Liquids and Gases, International Journal of Heat and Mass Transfer, 19, pp. 545-551.

Kays, W.M., Crawford, M.E., 1980. Convective Heat and Mass Transfer, 2nd edition, McGraw-Hill, New York, NY.

Paolucci, S., Chenoweth, D.R., 1987. Departures from the Boussinesq Approximation in Laminar Bénard Convection, Physics of Fluids, 30 (5), pp. 1561-1564.

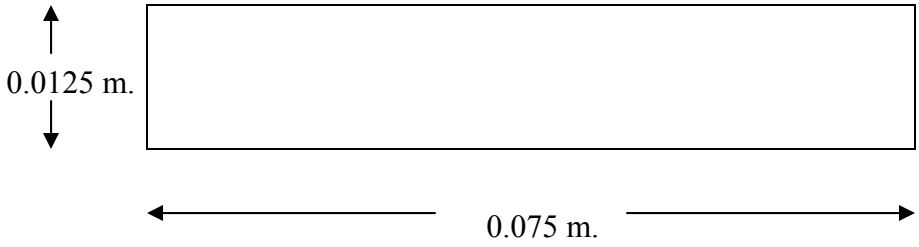

(a)

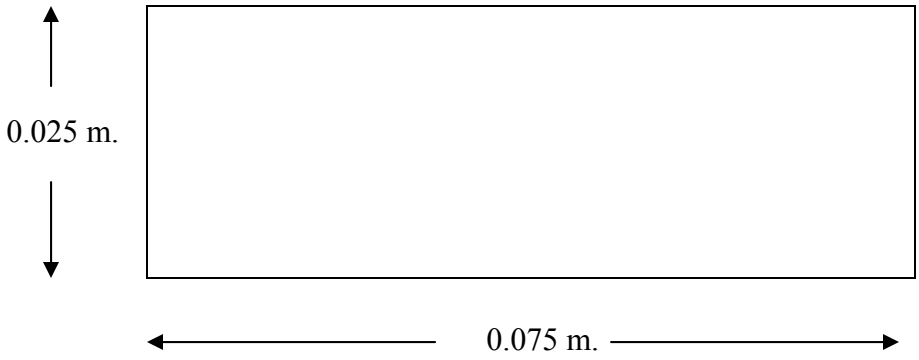

(b)

Fig. 1: Diagrams of configurations modeled for this paper. (a) case 1, (b) case 2, which is the same in length as case 1, but double the height.

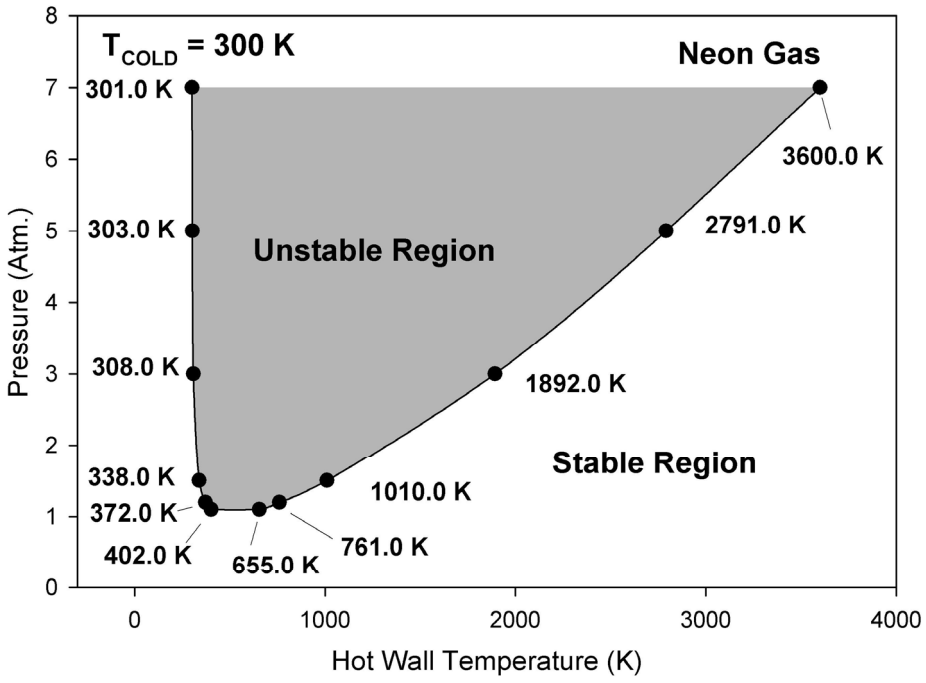

(a)

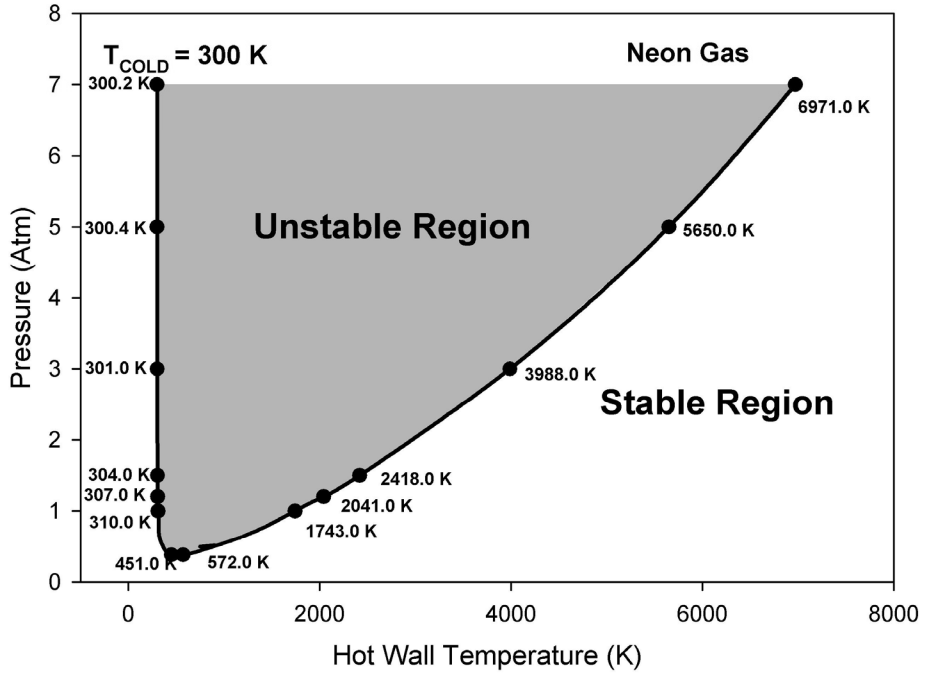

(b)

Fig.2: a) A schematic of calculated stable and unstable regions for neon for (a) case 1, (b) case 2. Hot surface temperatures at which transition occurs at various pressures are indicated.

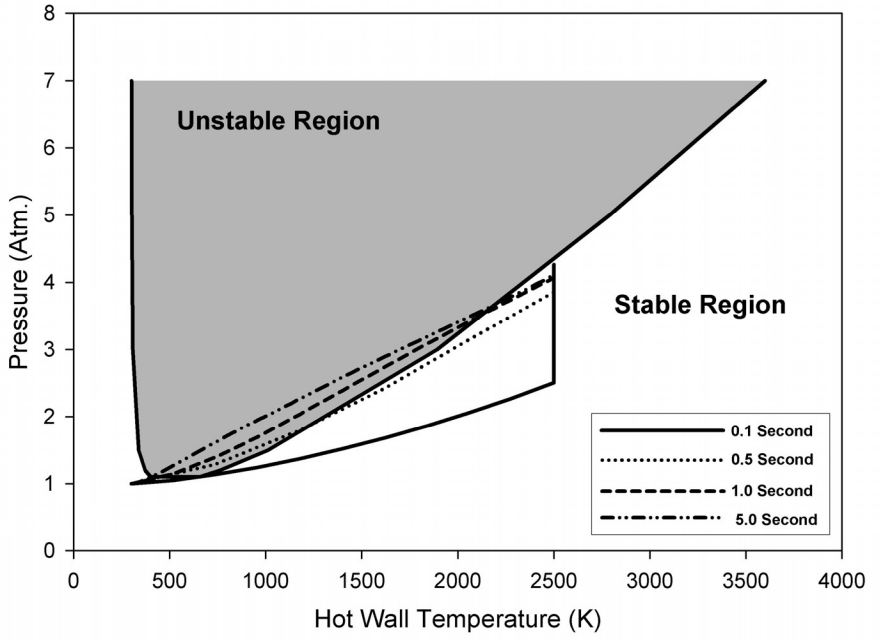

(a)

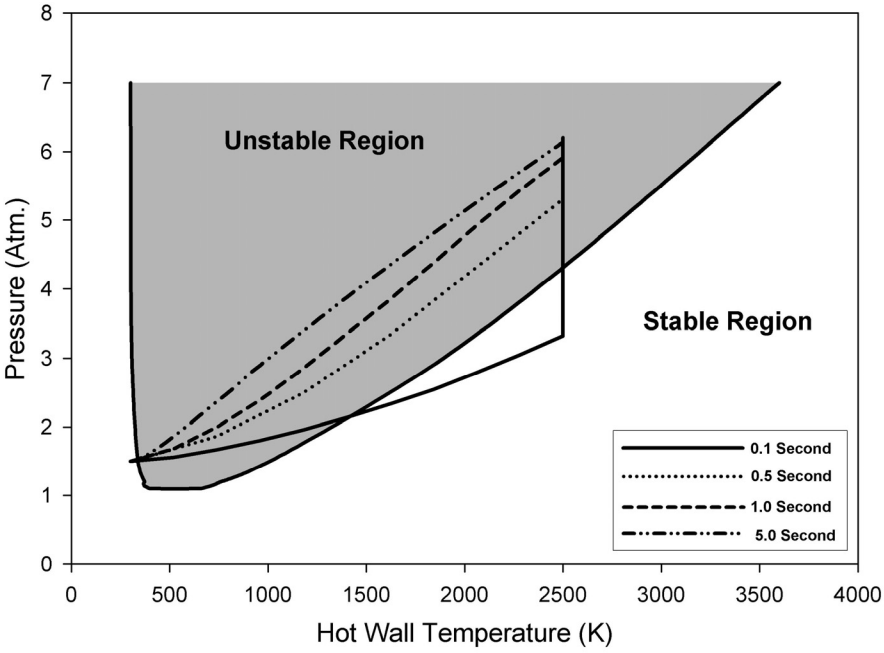

(b)

Fig.3: Case 1: pressure vs. hot wall temperature for various hot wall temperature ramp times, (a) P_i = 1.0 atm, (b) P_i = 1.5 atm.

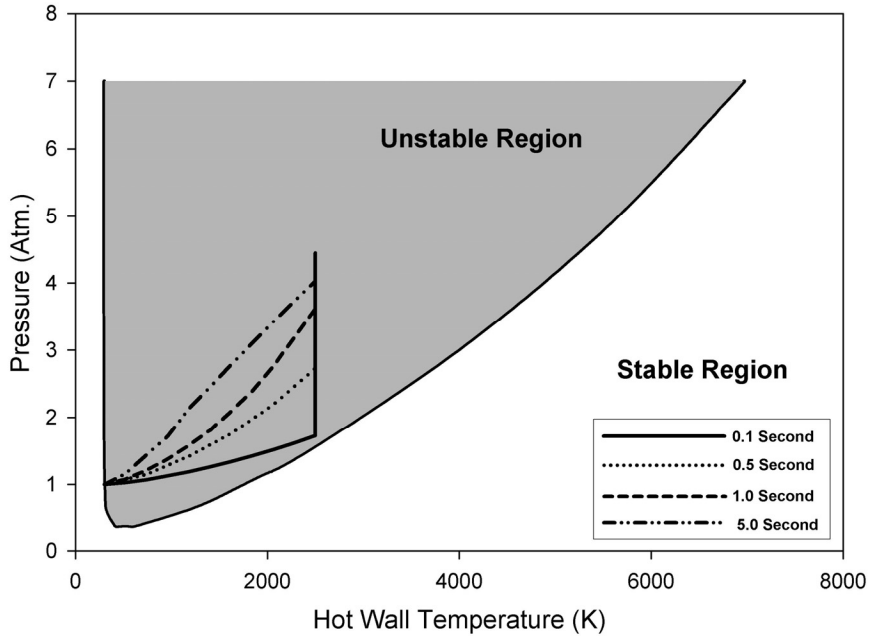

(a)

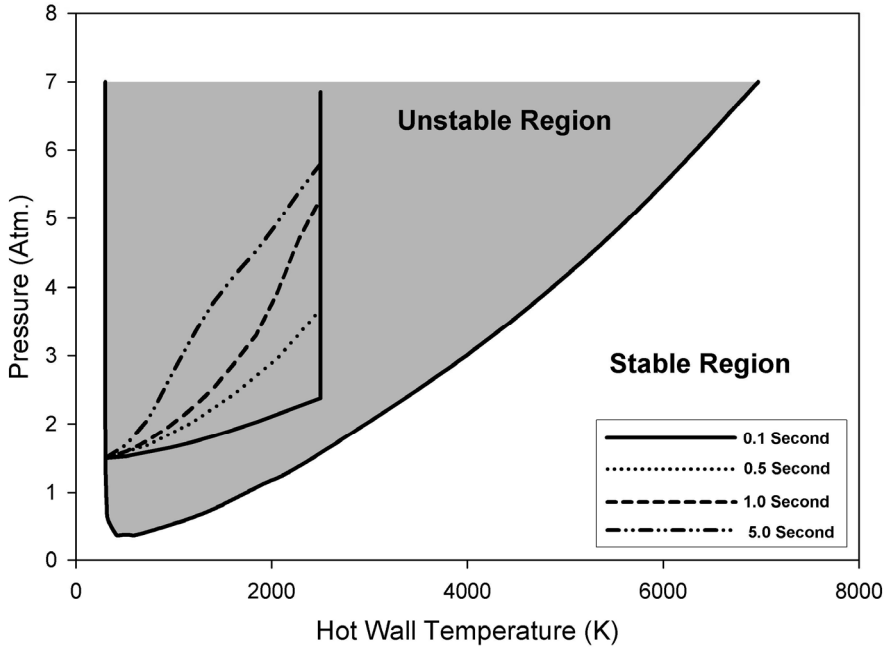

(b)

Fig.4: Case 2: pressure vs. hot wall temperature for various hot wall temperature ramp times, (a) P_i = 1.0 atm, (b) P_i = 1.5 atm.

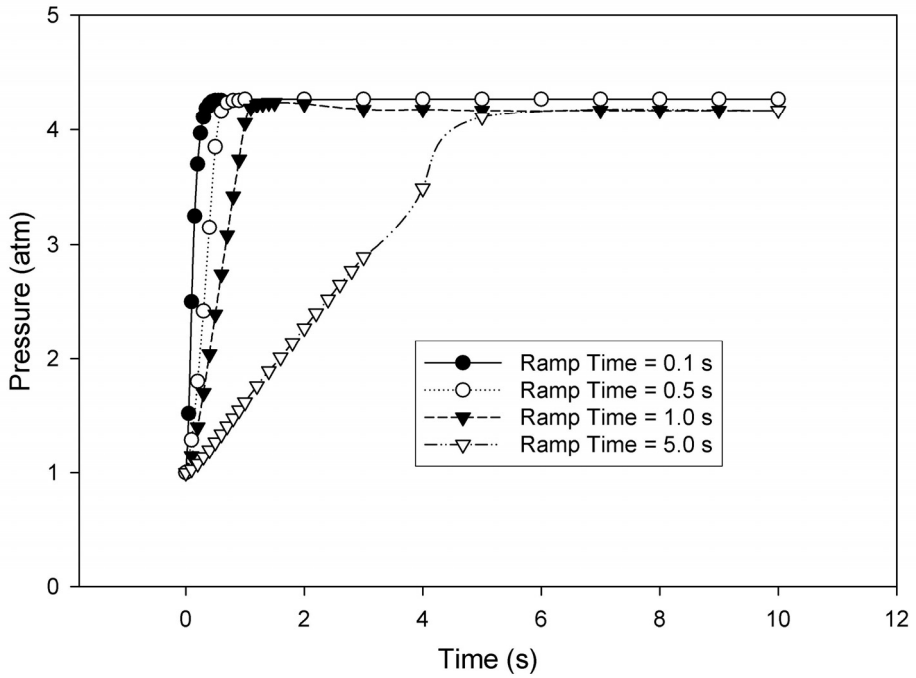

(a)

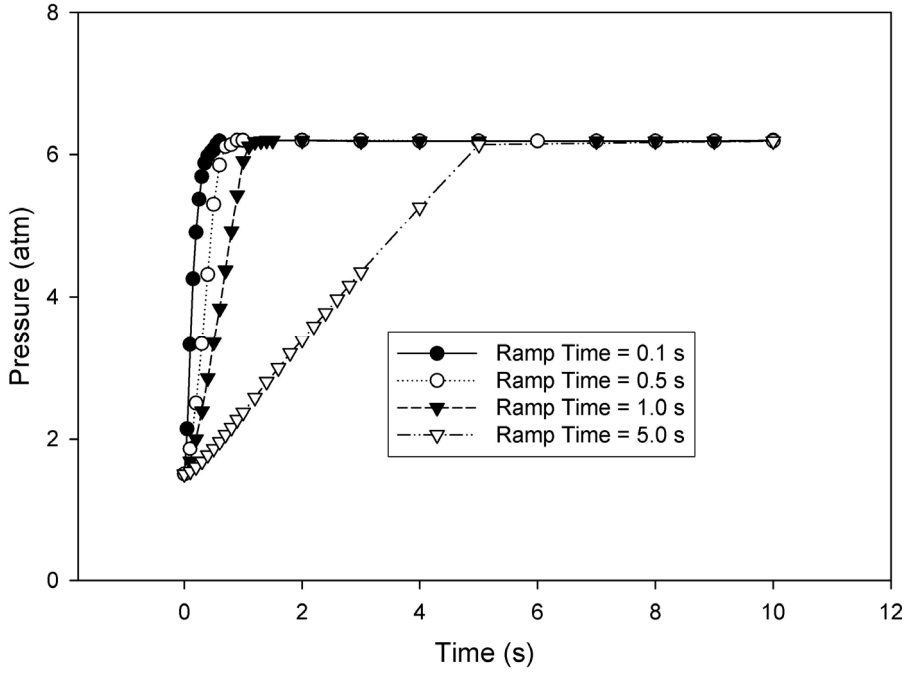

(b)

Fig.5: Case 1: pressure vs. time for various hot wall temperature ramp times, (a) P_i = 1.0 atm, (b) P_i = 1.5 atm. Note the different scales on the two plots.

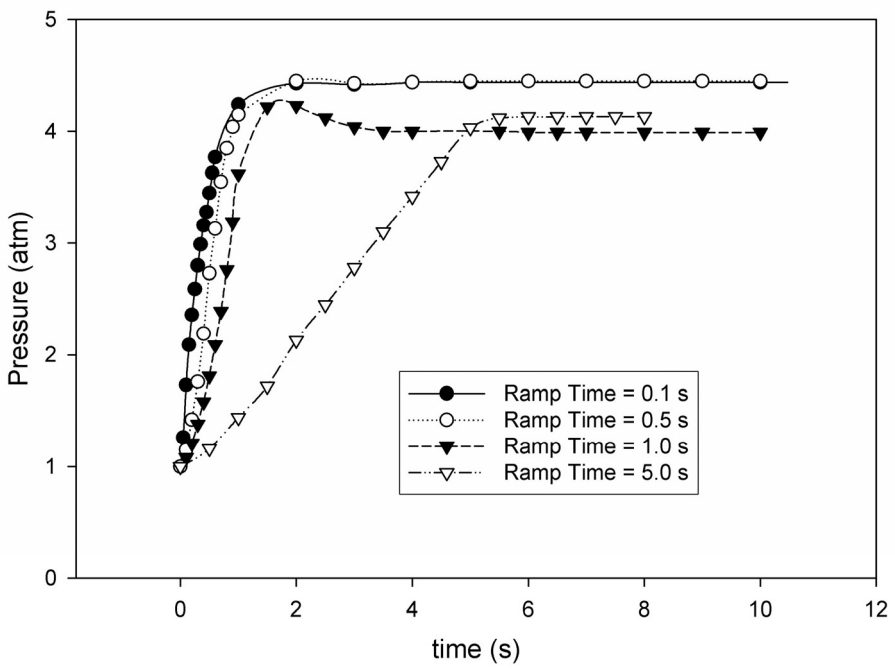

(a)

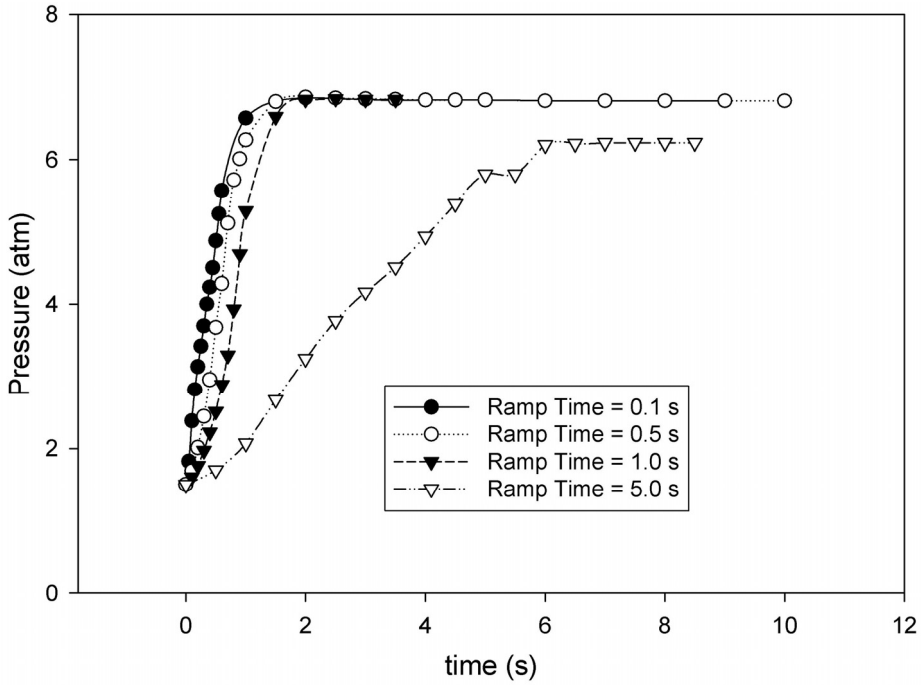

(b)

Fig.6: Case 2: pressure vs. time for various hot wall temperature ramp times, (a) P_i = 1.0 atm, (b) P_i = 1.5 atm. Note the different scales on the two plots.

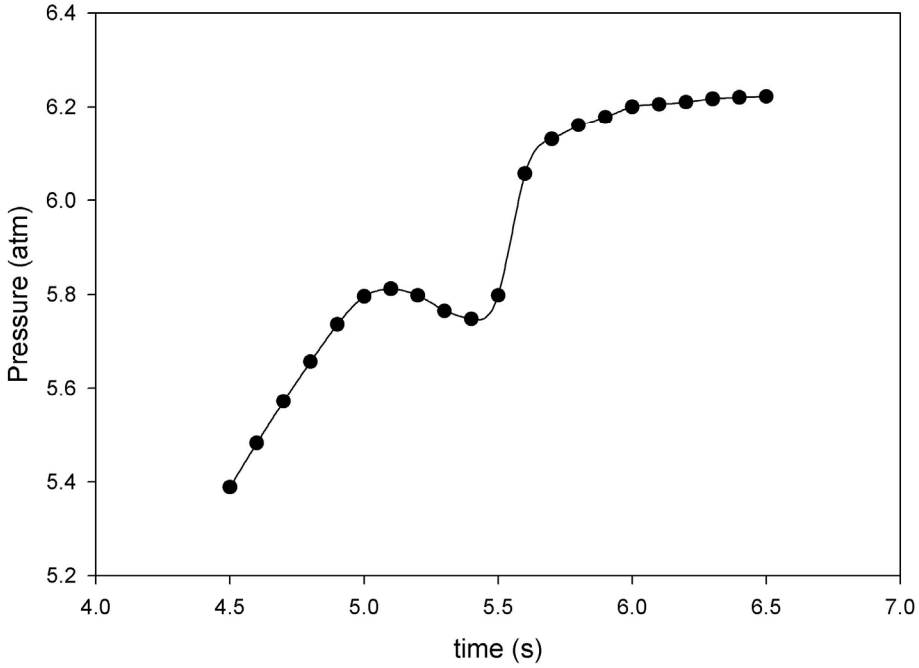

(a)

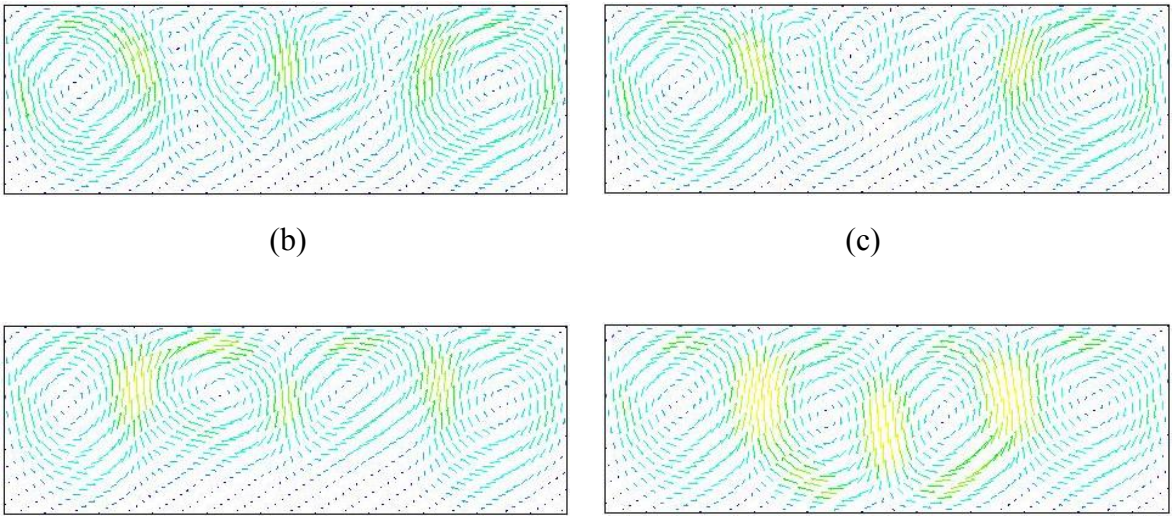

(b) (c)

(d) (e)

Fig.7: Case 2: (a) pressure vs. time for the five second temperature ramp between 4.5 and 6.5 s; velocity fields at: (b) 5.0 s, (c) 5.2 s, (d) 5.4 s, (e) 5.6 s.

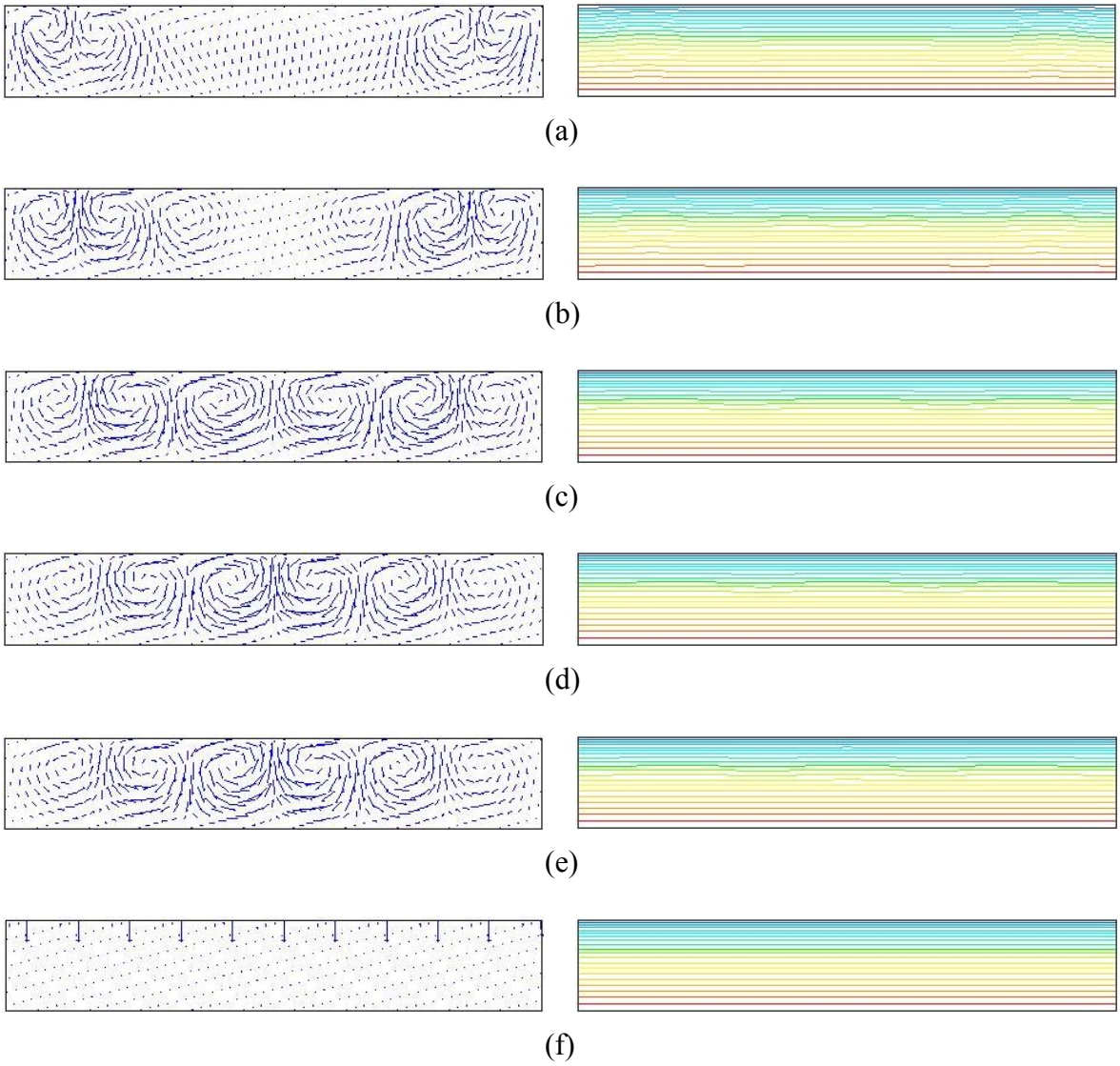

Fig. 8: Velocity and temperature fields in neon, case 1. Final T_h = 2500 K, P_i = 1.0 atm. Transient solution with a 0.1 second bottom wall temperature ramp after:
(a) 0.3 s (V_{max} =0.007 m/s), (b) 0.5 s (V_{max} = 0.004 m/s), (c) 2.0 s (V_{max} = 0.0007 m/s), (d) 5.0 s (V_{max} = 0.0006 m/s), (e) 10.0 s (V_{max} = 0.0006 m/s).; (f) steady state solution (V_{max} = 0.009 m/s). 0.5 second temperature ramp yields similar results.

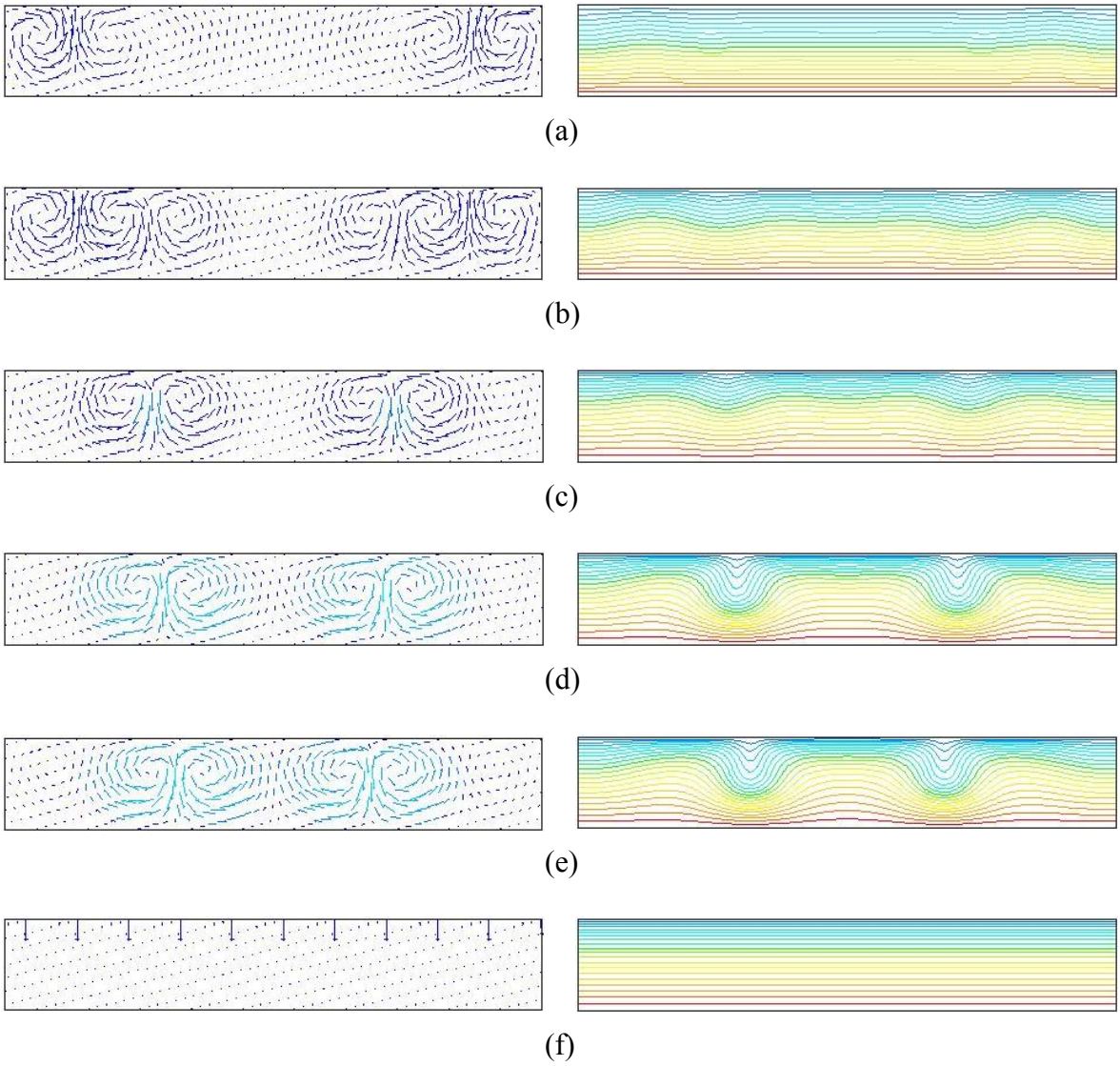

Fig. 9: Velocity and temperature fields in neon, case 1. Final T_h = 2500 K, P_i = 1.0 atm. Transient solution with a 1.0 second bottom wall temperature ramp after:
(a) 0.5 s (V_{max} =0.01 m/s), (b) 0.8 s (V_{max} = 0.02 m/s), (c) 1.5 s (V_{max} = 0.04 m/s), (d) 5.0 s (V_{max} = 0.1 m/s), (e) 10.0 s (V_{max} = 0.1 m/s).; (f) steady state solution (V_{max} = 0.0.009 m/s). 5.0 second temperature ramp yields similar results.

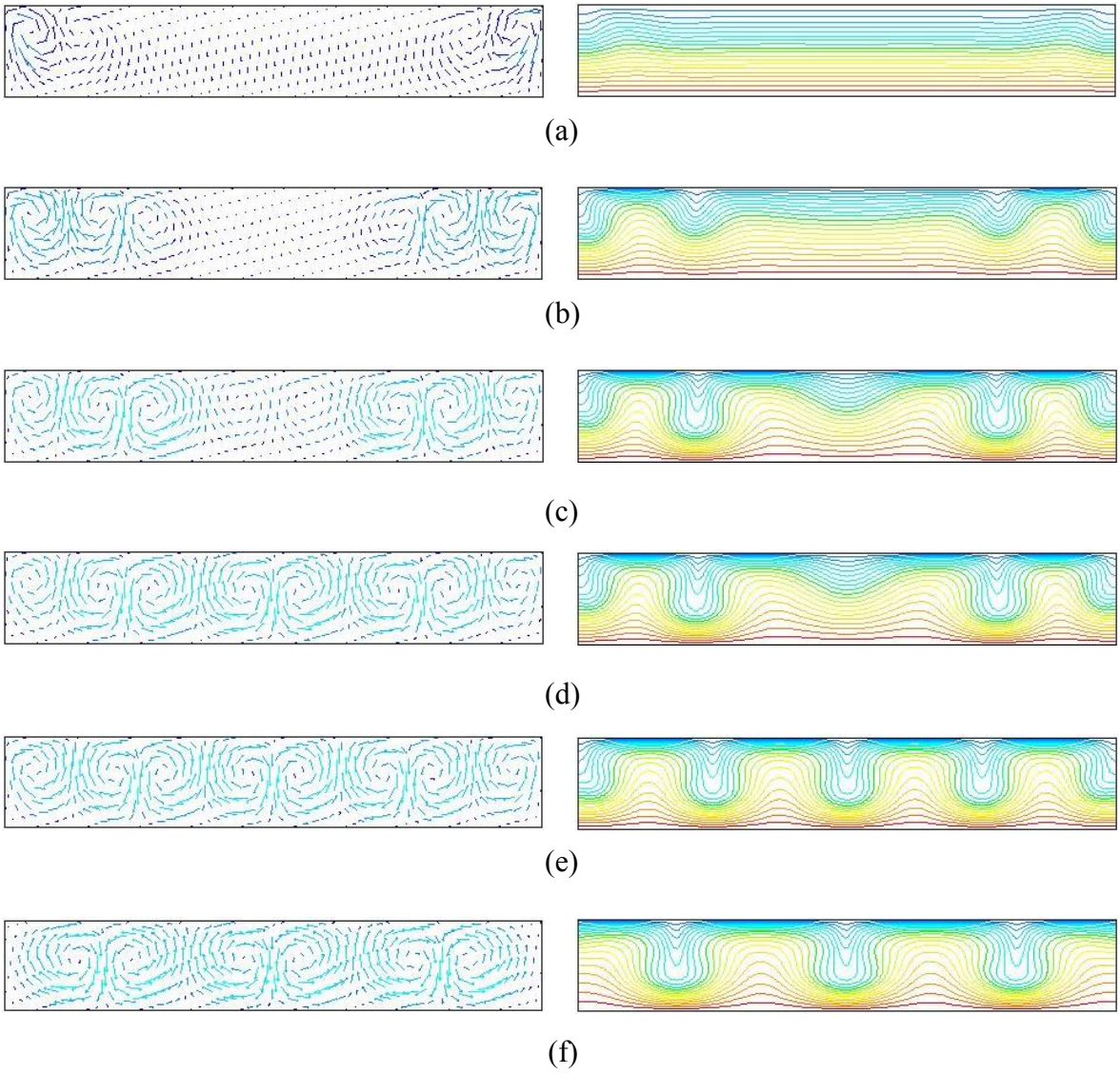

Fig. 10: Velocity and temperature fields in neon, case 1. Final T_h = 2500 K, P_i = 1.5 atm. Transient solution with a 0.1 second bottom wall temperature ramp after:
(a) 0.2 s (V_{max} =0.03 m/s), (b) 0.4 s (V_{max} = 0.09 m/s), (c) 0.6 s (V_{max} = 0.2 m/s), (d) 0.8 s (V_{max} = 0.2 m/s), (e) 10.0 s (V_{max} = 0.2 m/s).; (f) steady state solution (V_{max} = 0.2 m/s). 0.5 and 1.0 second temperature ramps yield similar results.

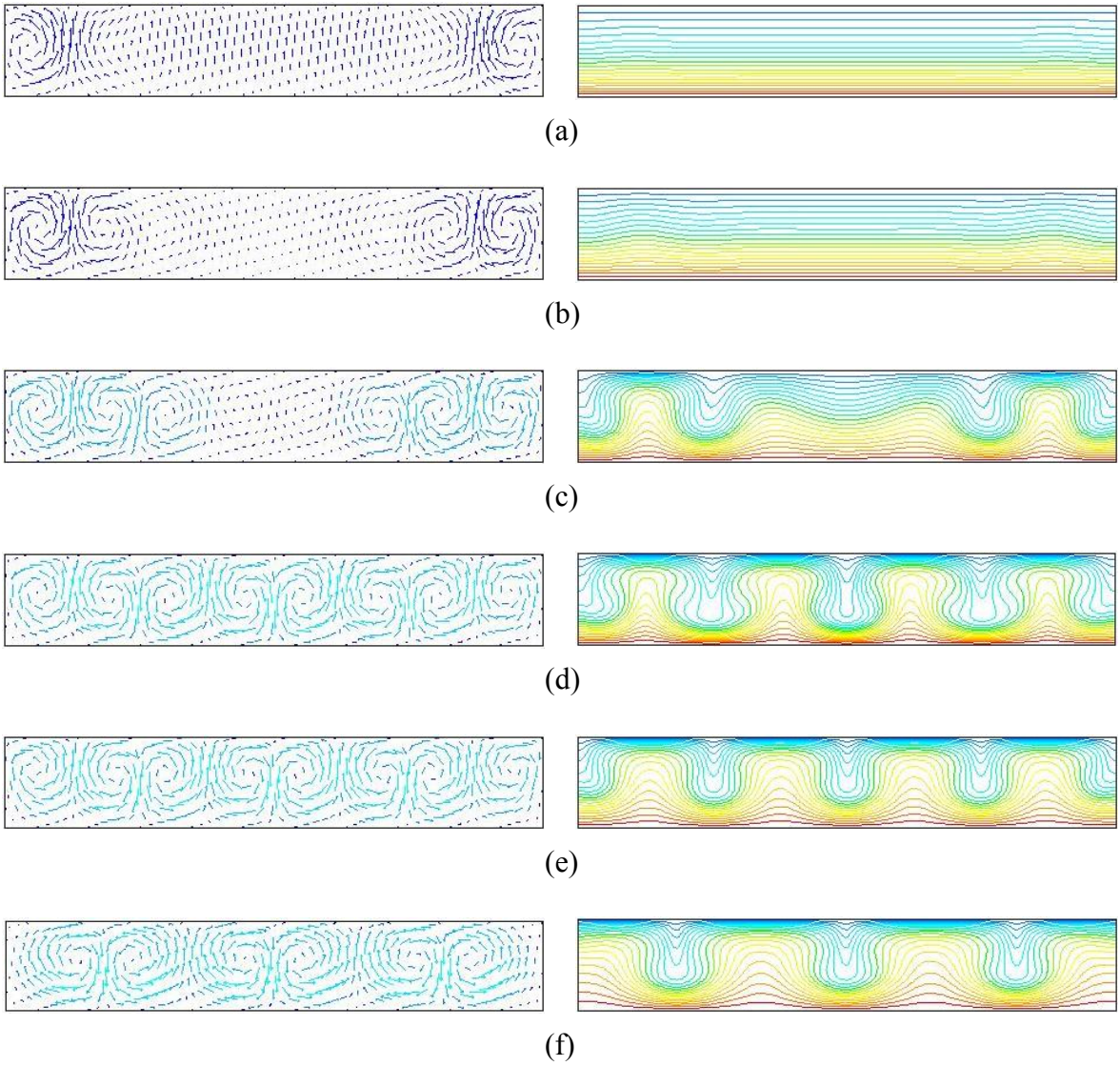

Fig. 11: Velocity and temperature fields in neon, case 1. Final T_h = 2500 K, P_i = 1.5 atm. Transient solution with a 5.0 second bottom wall temperature ramp after:
(a) 0.6 s (V_{max} =0.004 m/s), (b) 0.8 s (V_{max} = 0.01 m/s), (c) 1.1 s (V_{max} = 0.1 m/s), (d) 1.3 s (V_{max} = 0.2 m/s), (e) 10.0 s (V_{max} = 0.2 m/s).; (f) steady state solution (V_{max} = 0.2 m/s).

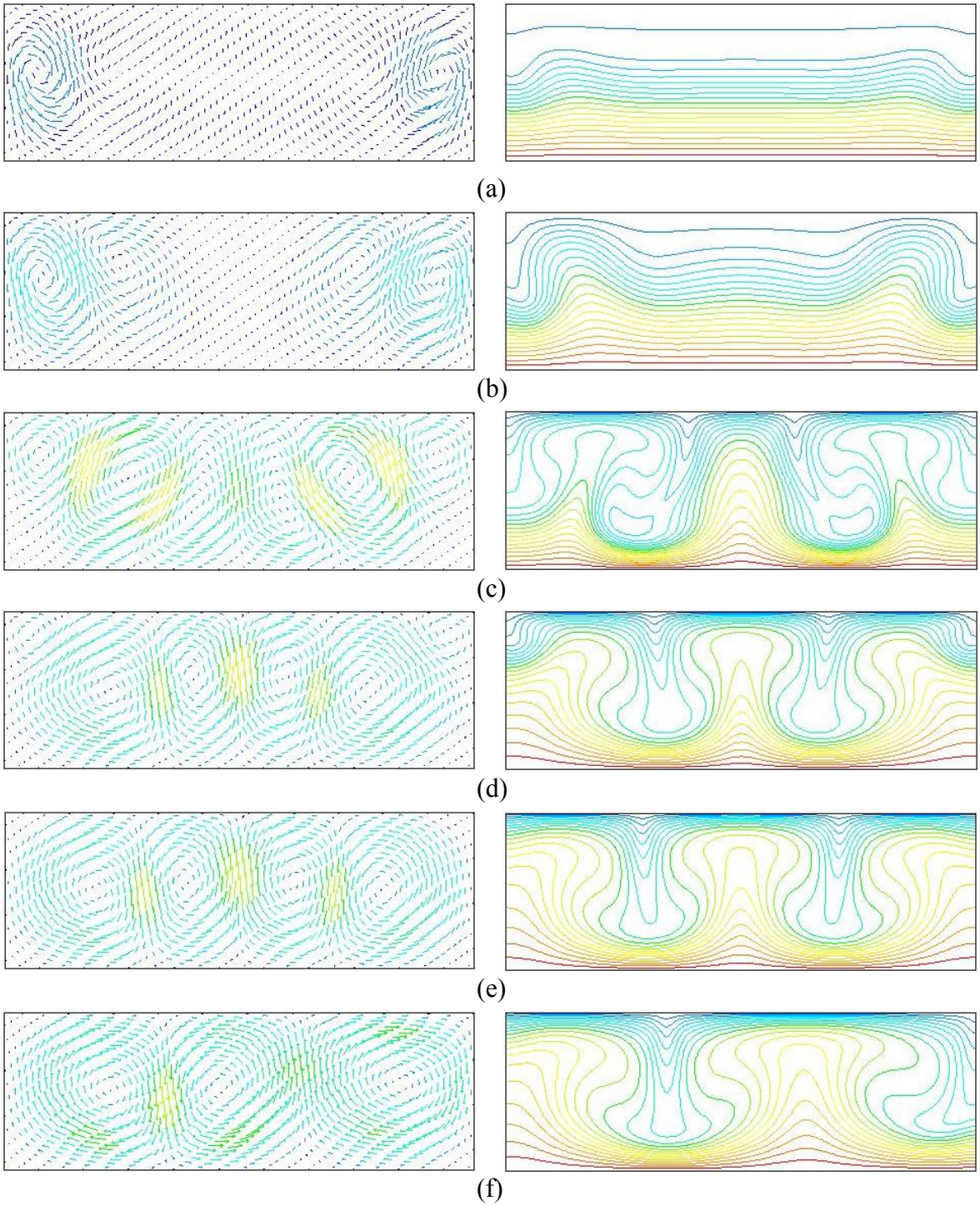

Fig. 12: Velocity and temperature fields in neon, case 2. Final T_h = 2500 K, P_i = 1.0 atm. Transient solution with a 0.1 second bottom wall temperature ramp after:
(a) 0.2 s (V_{max} =0.06 m/s), (b) 0.3 s (V_{max} = 0.2 m/s), (c) 0.5 s (V_{max} = 0.3 m/s), (d) 0.8 s (V_{max} = 0.3 m/s), (e) 10.0 s (V_{max} = 0.3 m/s).; (f) steady state solution (V_{max} = 0.3 m/s). 0.5 second temperature ramp yields similar results.

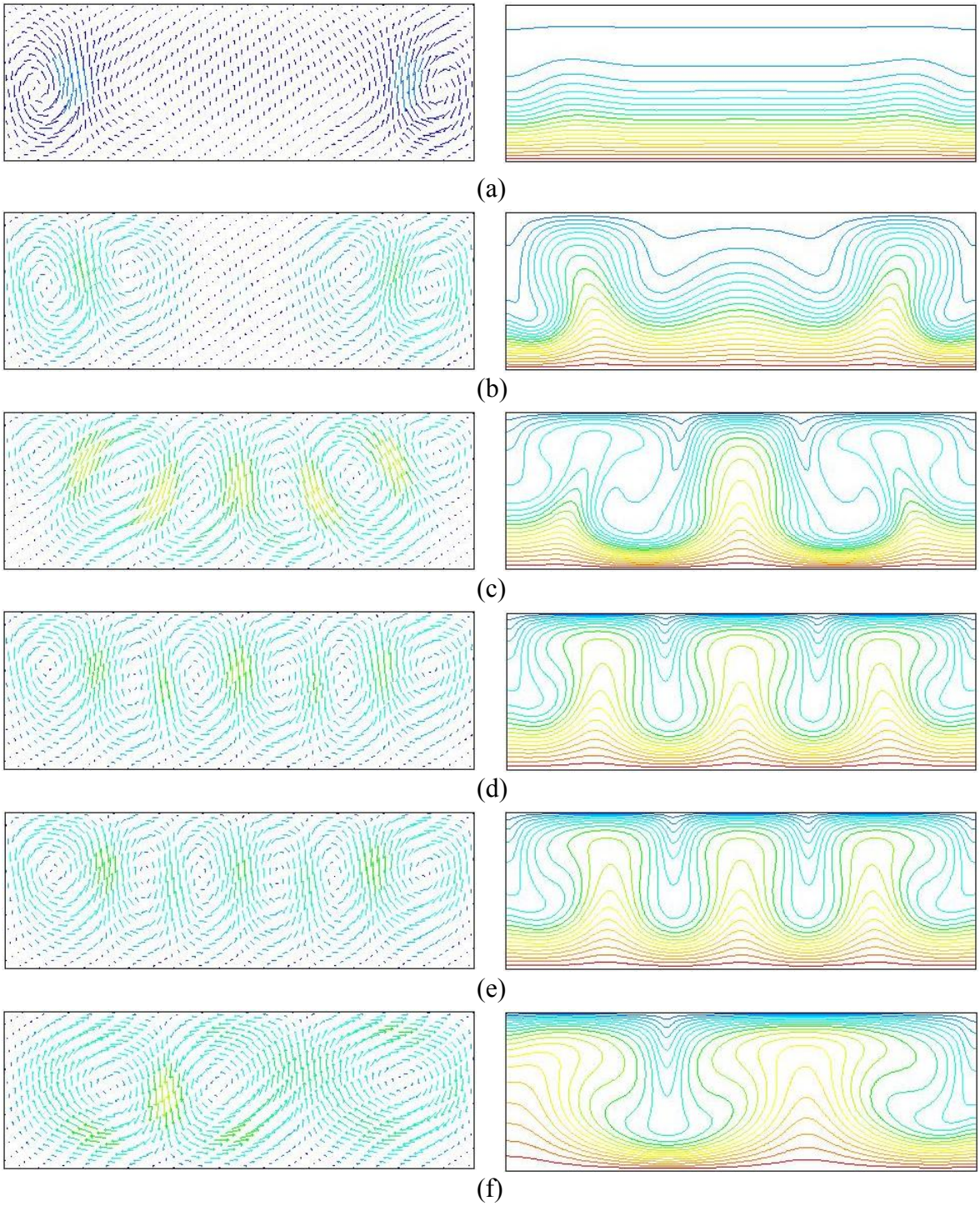

Fig. 13: Velocity and temperature fields in neon, case 2. Final T_h = 2500 K, P_i = 1.0 atm. Transient solution with a 1.0 second bottom wall temperature ramp after:
(a) 0.4 s (V_{max} =0.03 m/s), (b) 0.6 s (V_{max} = 0.2 m/s), (c) 0.8 s (V_{max} = 0.3 m/s), (d) 3.0 s (V_{max} = 0.3 m/s), (e) 10.0 s (V_{max} = 0.3 m/s).; (f) steady state solution (V_{max} = 0.3 m/s).

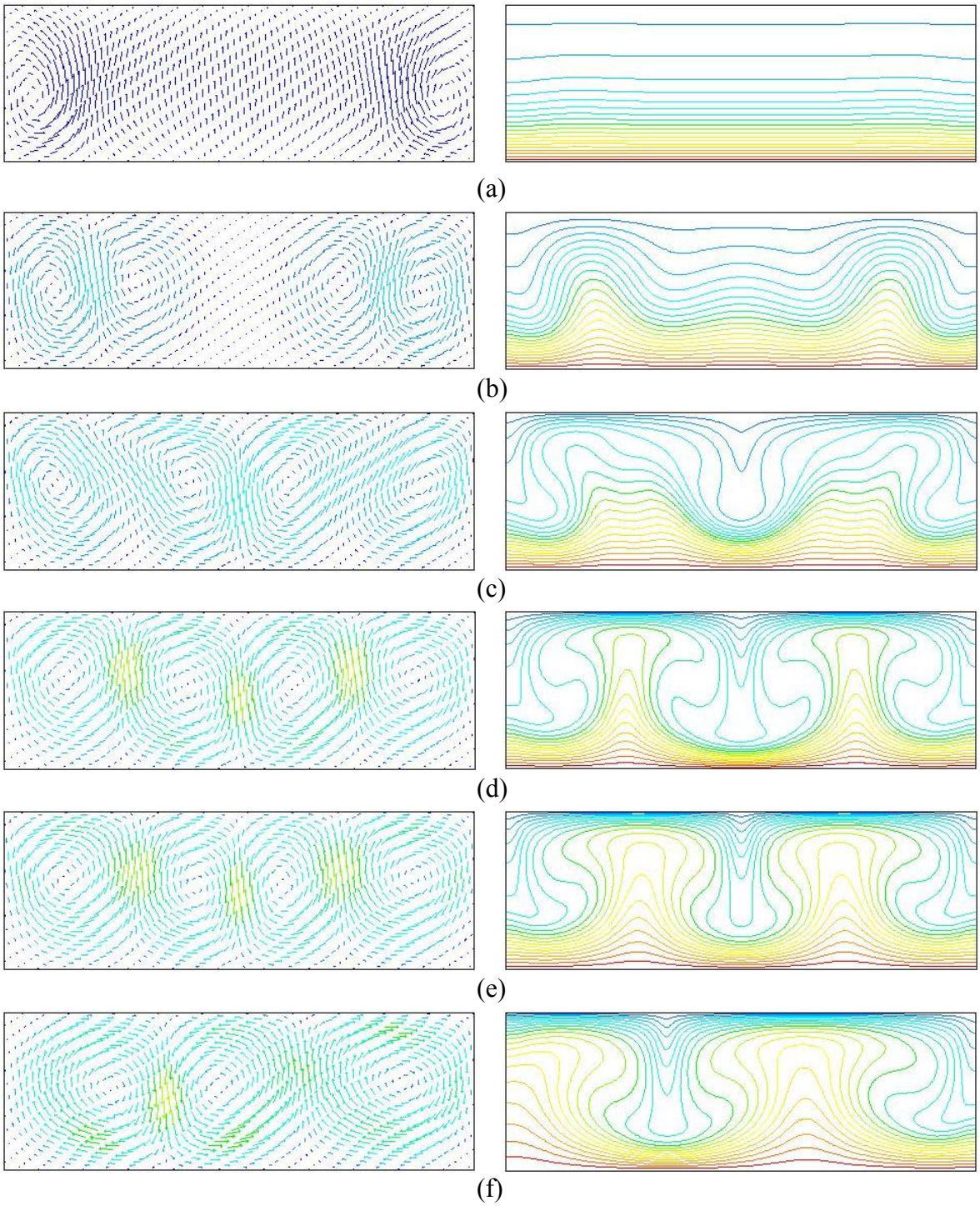

Fig. 14: Velocity and temperature fields in neon, case 2. Final T_h = 2500 K, P_i = 1.0 atm. Transient solution with a 5.0 second bottom wall temperature ramp after:
(a) 0.6 s (V_{max} =0.006 m/s), (b) 1.0 s (V_{max} = 0.1 m/s), (c) 1.5 s (V_{max} = 0.2 m/s), (d) 2.0 s (V_{max} = 0.3 m/s), (e) 10.0 s (V_{max} = 0.3 m/s).; (f) steady state solution (V_{max} = 0.3 m/s).

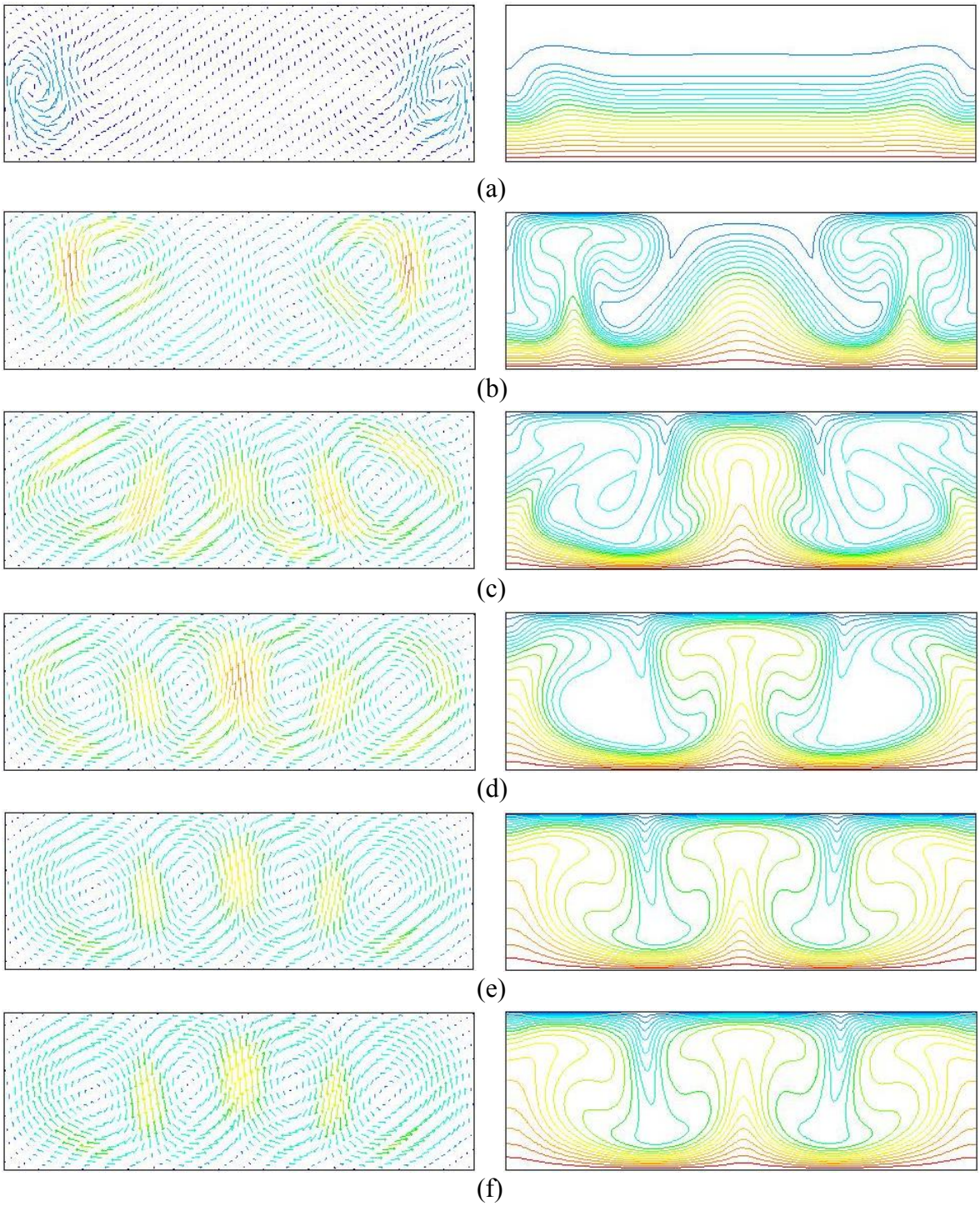

Fig. 15: Velocity and temperature fields in neon, case 2. Final T_h = 2500 K, P_i = 1.5 atm. Transient solution with a 0.1 second bottom wall temperature ramp after:
(a) 0.2 s (V_{max} =0.07 m/s), (b) 0.4 s (V_{max} = 0.5 m/s), (c) 0.5 s (V_{max} = 0.4 m/s), (d) 0.6 s (V_{max} = 0.4 m/s), (e) 10.0 s (V_{max} = 0.4 m/s).; (f) steady state solution (V_{max} = 0.4 m/s). 0.5 second temperature ramp yields similar results.

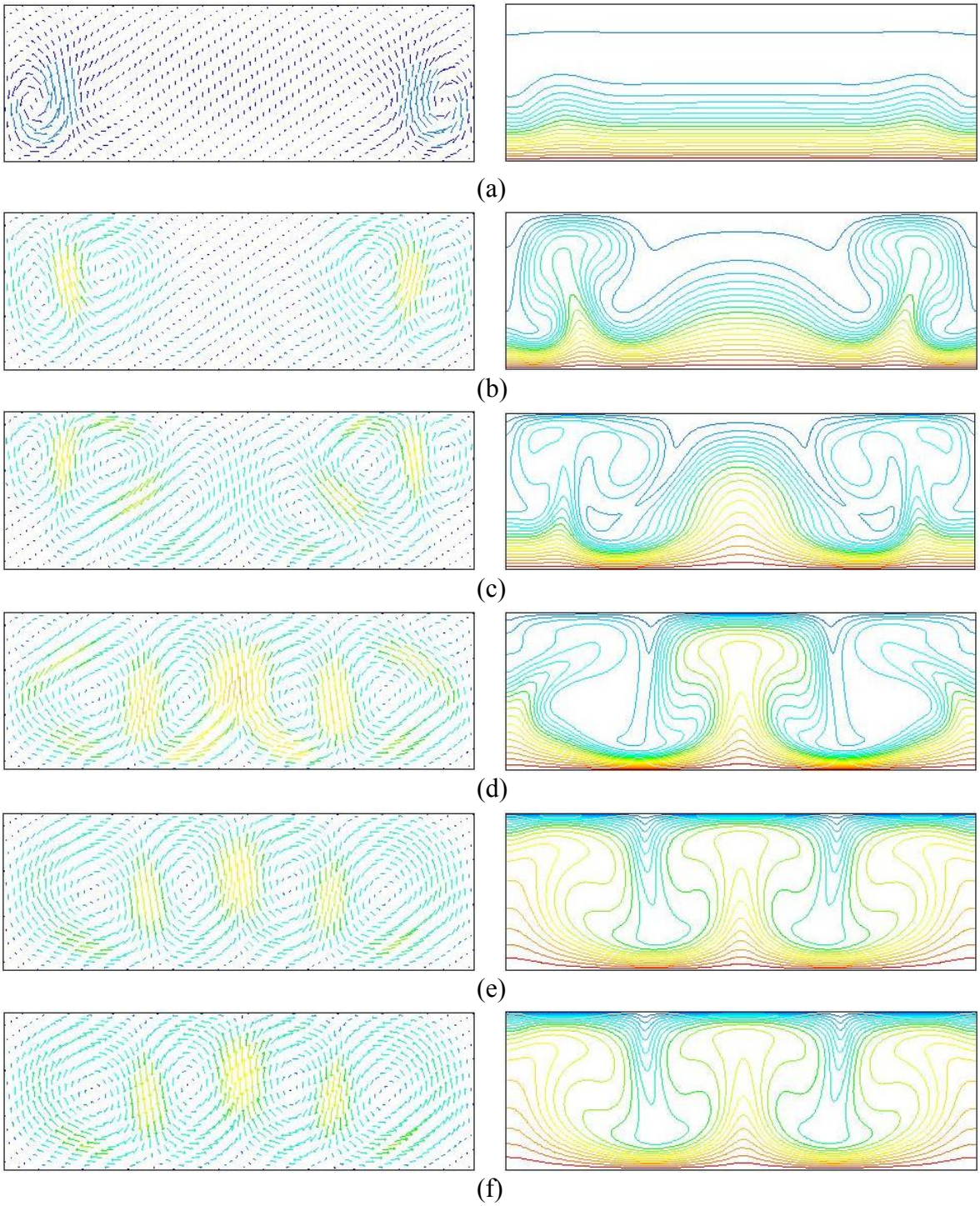

Fig. 16: Velocity and temperature fields in neon, case 2. Final T_h = 2500 K, P_i = 1.5 atm. Transient solution with a 1.0 second bottom wall temperature ramp after:
(a) 0.4 s (V_{max} =0.04 m/s), (b) 0.6 s (V_{max} = 0.4 m/s), (c) 0.7 s (V_{max} = 0.3 m/s), (d) 0.8 s (V_{max} = 0.4 m/s), (e) 10.0 s (V_{max} = 0.4 m/s).; (f) steady state solution (V_{max} = 04 m/s).

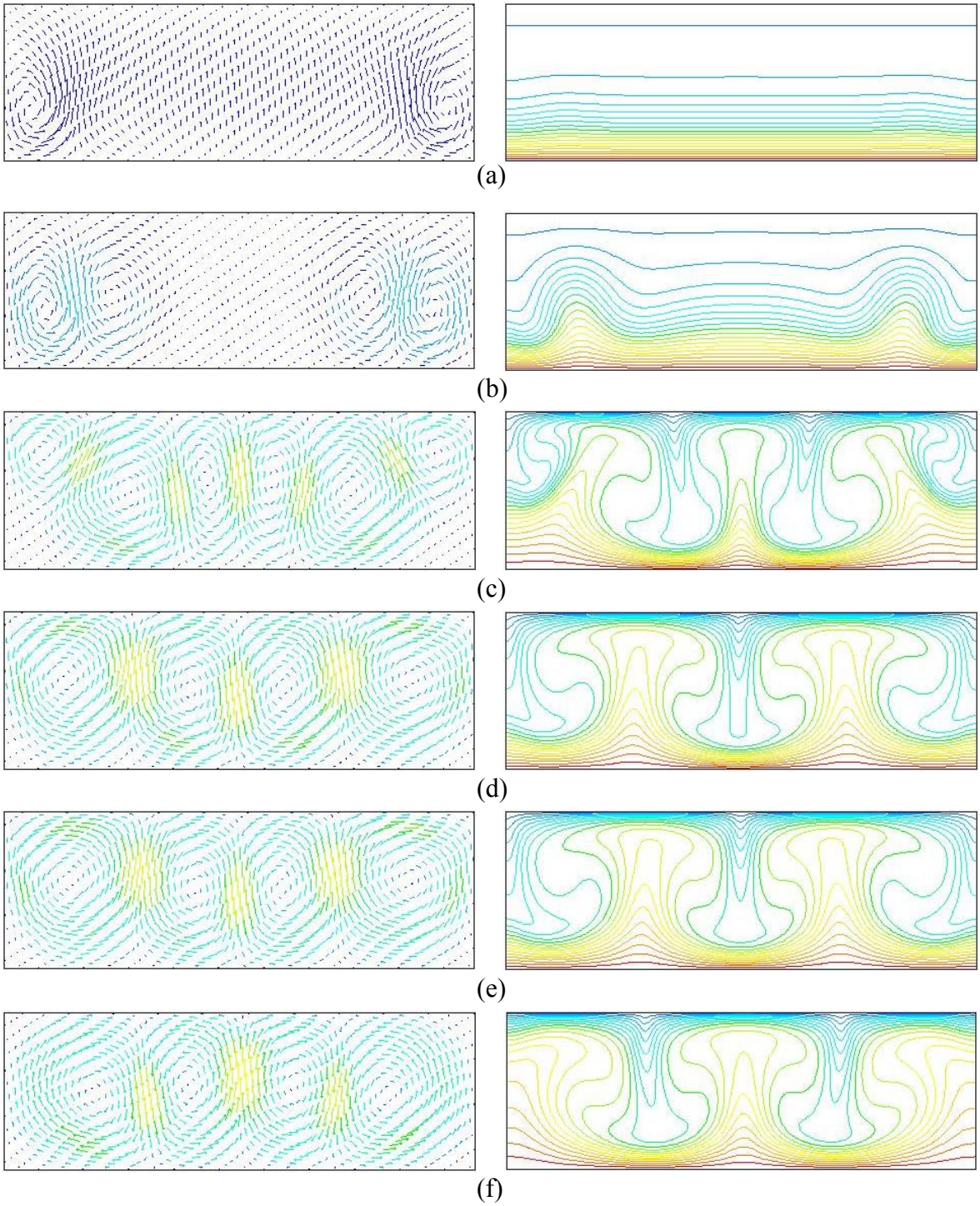

Fig. 17: Velocity and temperature fields in neon, case 2. Final T_h = 2500 K, P_i = 1.5 atm. Transient solution with a 5.0 second bottom wall temperature ramp after:
(a) 0.6 s (V_{max} =0.008 m/s),(b) 0.9 s (V_{max} = 0.09 m/s), (c) 3.0 s (V_{max} = 0.3 m/s), (d) 6.0 s (V_{max} = 0.3 m/s), (e) 10.0 s (V_{max} = 0.3 m/s).; (f) steady state solution (V_{max} = 0.3 m/s).

Table 1
Grid Sensitivity Study Results

grid	# cells in X	# cells in Y	% change in Q (J/s)
grid 0	60	10	
grid 1	120	20	(Q1-Q0)/Q0 = 0.03
grid 2	240	40	(Q2-Q1)/Q1 = 0.009
grid 3	480	80	(Q3-Q2)/Q2 = 0.002

Table 2
Comparison of Final Pressure Predicted by the Ideal Gas Law and FLUENT

Case	P_i (atm)	Ramp time (sec)	P_f (atm.) Ideal gas law	P_f (atm.) FLUENT	% difference
1	1.0	0.1	4.67	4.27	- 8.6
1	1.0	0.5	4.67	4.27	- 8.6
1	1.0	1.0	4.67	4.17	-10.7
1	1.0	5.0	4.67	4.17	-10.7
1	1.5	0.1	7.0	6.20	-11.4
1	1.5	0.5	7.0	6.19	-11.6
1	1.5	1.0	7.0	6.19	-11.6
1	1.5	5.0	7.0	6.19	-11.6
2	1.0	0.1	4.67	4.45	- 4.7
2	1.0	0.5	4.67	4.45	- 4.7
2	1.0	1.0	4.67	3.99	-14.6
2	1.0	5.0	4.67	4.13	-11.6
2	1.5	0.1	7.0	6.81	- 2.7
2	1.5	0.5	7.0	6.81	- 2.7
2	1.5	1.0	7.0	6.81	- 2.7
2	1.5	5.0	7.0	6.23	-11.0